Chemical Physics Letters 459 (2008) 141–145

Contents lists available at ScienceDirect

Chemical Physics Letters

journal homepage: www.elsevier.com/locate/cplett

Inflection in the loading dependence of the Maxwell–Stefan diffusivity of *iso*-butane in MFI zeolite

C. Chmelik [a], L. Heinke [a], J. Kärger [a], W. Schmidt [b], D.B. Shah [c], J.M. van Baten [d], R. Krishna [d,*]

[a] Abteilung Grenzflächenphysik, Universität Leipzig, Linnéstraße 5, 04103 Leipzig, Germany
[b] Max Planck Institute for Coal Science, Kaiser-Wilhelm-Platz 1, D-45470 Mülheim, Germany
[c] Department of Chemical and Biomedical Engineering, Cleveland State University, 2121 Euclid Avenue, Cleveland, OH 44115, USA
[d] Van 't Hoff Institute for Molecular Sciences, University of Amsterdam, Nieuwe Achtergracht 166, 1018 WV Amsterdam, The Netherlands

ARTICLE INFO

Article history:
Received 3 March 2008
In final form 14 May 2008
Available online 20 May 2008

ABSTRACT

Configurational-bias Monte Carlo simulations of the adsorption isotherm for *iso*-butane (iC4) in MFI zeolite shows a strong inflection at a loading $\Theta = 4$ molecules per unit cell. The consequence of the isotherm inflection on the loading dependence of the Maxwell–Stefan (M–S) diffusivity, $Đ$, was investigated using infra-red microscopy (IRM). The experimental data show that $Đ$ decreases nearly linearly as Θ is increased to 4; further increase in Θ results in a sharp increase in $Đ$, with a cusp at $\Theta = 4$. Kinetic Monte Carlo (KMC) simulations are used to rationalize the experimental observations. The simulations indicate that significant inter-molecular repulsions are present for $\Theta > 4$.

1. Introduction

Zeolites are widely used as adsorbents and catalysts in a variety of applications in the chemical and petrochemical industries. For the design of separation processes employing zeolites it is necessary to have accurate information on the transport, or Fick diffusivity D of guest molecules [1]. For zeolite catalysed reactions, the calculation of the catalyst effectiveness factor requires knowledge of D [2,3]. The Fick diffusivity is defined for one-component diffusion by $N = -\rho D \frac{d\Theta}{dx}$ where N is the molecular flux, Θ is molecular loading expressed in molecules per unit cell, ρ is the zeolite framework density, expressed as the number of unit cells per m^3, and the Fick diffusivity D has the units of $m^2\ s^{-1}$. In the alternative Maxwell–Stefan (M–S) approach [4–8] the chemical potential gradient $d\mu/dx$ is used as the driving force and the M–S diffusivity $Đ$ is defined by $N = -\rho\Theta(Đ/RT)d\mu/dx$ where R is the gas constant, and T is the absolute temperature. The Fick and M–S diffusivities are inter-related, $Đ = D/\Gamma$, where Γ is the thermodynamic correction factor, $\Gamma \equiv d\ln p/d\ln\Theta$. The thermodynamic factor Γ can be determined from knowledge of the adsorption isotherm that relates the molecular loading Θ to the bulk gas phase pressure p.

In recent years, there has been increasing experimental evidence [7–10] that the M–S diffusivity $Đ$ is dependent on the loading Θ. In the case of MFI zeolite, the $Đ$–Θ dependence appears to be related to the dependence of $1/\Gamma$ on Θ [4–8]. For adsorption of branched alkanes, for example *iso*-butane (iC4), 2-methylpentane, and 3-methylpentane, and benzene in MFI, the isotherm exhibits a strong inflection at a loading $\Theta = 4$. As an example, CBMC simulations for the adsorption isotherm for iC4 in MFI at 298 K are shown in Fig. 1a (see Supplementary material for the the simulation methodology and details). The CBMC simulations are in good agreement with the experimental data reported by Zhu et al. [11]. The isotherm inflection is caused due to preferential location of the iC4 at the intersections between the straight and zig–zag channels. Fig. 2a,b show snapshots of the location of iC4 molecules at loadings of 2 and 6 molecules per unit cell. We note that for $\Theta \leqslant 4$, iC4 locates at the intersections exclusively. For $\Theta = 4$, all the intersection sites are occupied and further increase in the loading is achieved only with an extra 'push', resulting in an isotherm inflection [12–15]. For $\Theta \geqslant 4$, iC4 locates within the channel interiors; see Fig. 2b. The dual-site Langmuir (DSL) isotherm $\Theta(p) \equiv \Theta_A + \Theta_B$; $\Theta_A = \Theta_{sat,\,A} b_A p/(1 + b_A p)$; $\Theta_B = \Theta_{sat,\,B} b_B p/(1 + b_B p)$ provides a good description of the adsorption isotherm. Here b_A and b_B represent the DSL model parameters and the subscripts A and B refer to two sorption sites within the MFI structure, with different sorption capacities and sorption strengths. The $\Theta_{sat,A}$ and $\Theta_{sat,B}$ represent the saturation capacities of sites A and B, respectively. The fitted DSL model parameters are specified in Table 1. The inverse of the thermodynamic factor Γ is $1/\Gamma = \Theta_A/\Theta(1 - \Theta_A/\Theta_{sat,\,A}) + \Theta_B/\Theta(1 - \Theta_B/\Theta_{sat,B})$; Fig. 1b shows the variation of $1/\Gamma$ with Θ for iC4 in MFI.

Kinetic Monte Carlo (KMC) and molecular dynamics (MD) simulations have shown that if Γ vs. Θ exhibits a strong inflection, this is reflected in a corresponding inflection in $Đ$ vs. Θ [4–7]. The only experimental confirmation available for the anticipated inflection behavior is due to QENS measurements of Jobic et al. [8] for *n*-hexane and *n*-heptane in MFI; the observed inflection behavior is

* Corresponding author. Fax: +31 20 5255604.
E-mail address: r.krishna@uva.nl (R. Krishna).

0009-2614/$ - see front matter © 2008 Elsevier B.V. All rights reserved.
doi:10.1016/j.cplett.2008.05.023

however mild. Zhu et al. [16] have reported diffusivities for iC4 at loadings $\Theta < 4$ in MFI, and consequently no inflection could be detected. The primary objective of the present communication is to seek experimental confirmation, using infra-red microscopy (IRM), of the anticipated inflection in $Đ$ vs. Θ dependence for iC4 in MFI. The current investigation is an extension of previous work [17], wherein diffusivities were measured only up to loadings of 4.5 molecules per unit cell. In the current investigation additional measurements were made for the range of loadings 4.5–8.4 molecules per unit cell with the objective of capturing the inflection characteristics.

2. Infra-red microscopy experiments

The complete details of the experimental set-up, measurement procedure, data analysis and fitting of the uptake curves are available in the Supplementary Material. Some salient points are given below.

The experimental set-up consisted of an IR microscope; see Fig. 3. At first, several hundred crystals were introduced into the IR cell and activated. Then, in the viewing mode of the microscope, one particular zeolite crystal was selected by moving the motorized sample platform and adjusting the aperture accordingly (see Fig. 3). The rectangular aperture selects the region in the field of view which is scanned by IR light. Here, the size was set to about $100 \times 220\ \mu m^2$. All measurements were preformed in the IR-transmittance mode of the microscope. Prior to the uptake experiments,

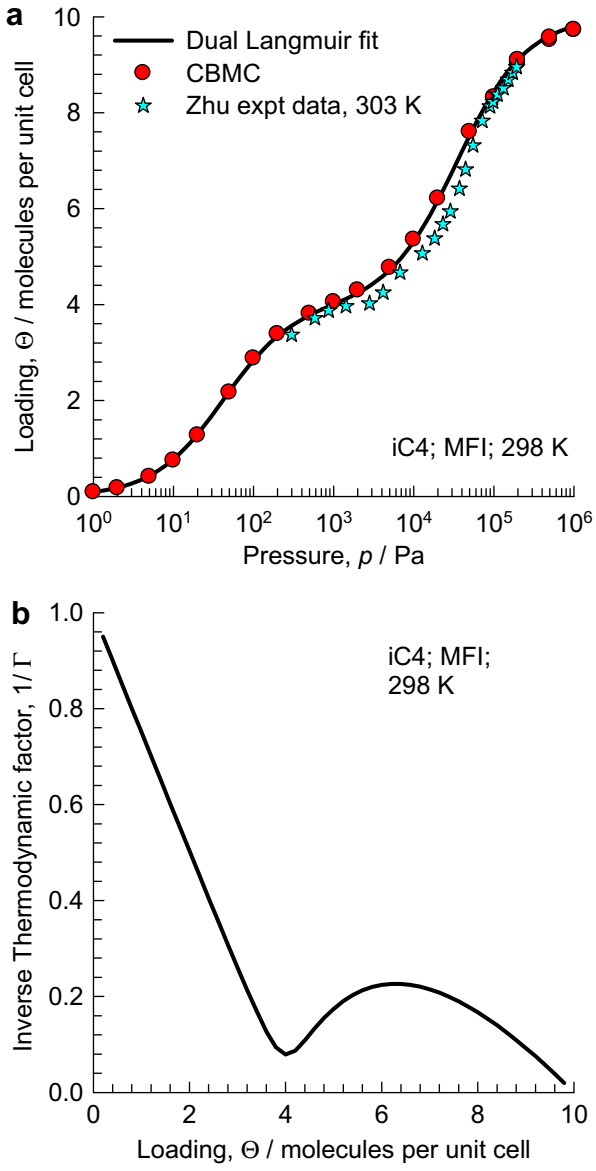

Fig. 1. (a) CBMC simulations (filled circles) of the adsorption isotherms for iC4 in MFI at 298 K. Also shown are the experimental data of Zhu et al. [11] at 303 K. The continuous solid lines represent the dual-site Langmuir (DSL) fits of the CBMC simulated isotherms with the parameter values specified in Table 1. (b) The inverse thermodynamic correction factor, $1/\Gamma$, as a function of the loading of iC4 in MFI.

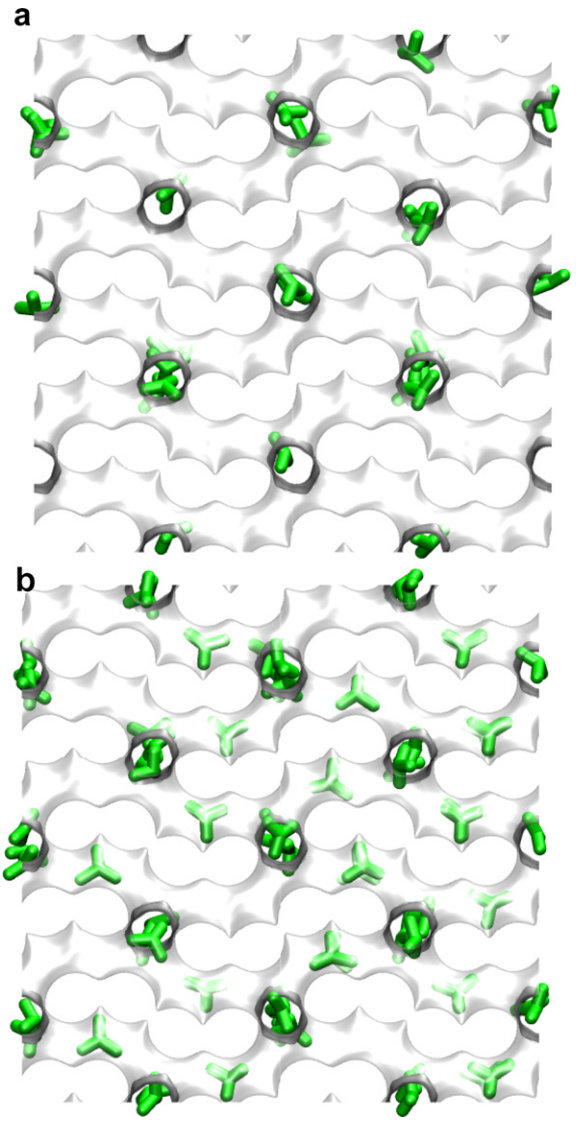

Fig. 2. Snapshots showing location of iC4 at loadings of (a) 2 and (b) 6 molecules per unit cell in MFI. The view is 2 unit cells deep.

Table 1
Dual-site Langmuir parameters for iC4 in MFI at 298 K

b_A	$\Theta_{sat,A}$	b_B	$\Theta_{sat,B}$
2.4×10^{-2}	4	2.85×10^{-5}	6

The saturation capacity, q_{sat}, has the units of molecules per unit cell. The Langmuir parameters, b, have the units of Pa^{-1}.

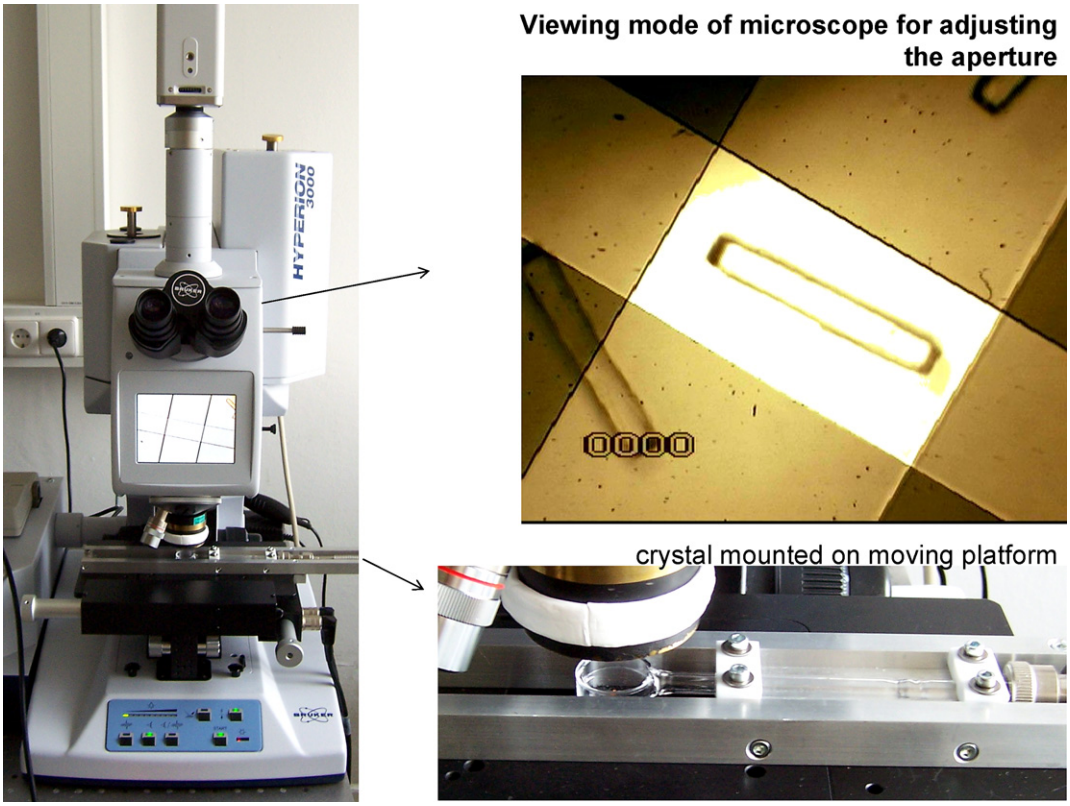

Fig. 3. Photograph of the IRM experimental set-up. The upper-right picture depicts the crystal observed with the microscope set in the viewing model. The bottom-right picture is a close-up of the motorized platform on which the crystal is placed.

the crystal was checked for anomalies in the IR spectrum, e.g. present C–H or water bands, to exclude a non-proper activation.

To follow the uptake of iC4 within the crystal, absorption spectra were recorded with a temporal resolution between 0.2 and 1.5 s. The spectral resolution was set to 16 cm^{-1}. The area under the C–H stretching band, enclosed by a straight baseline between 2800 and 3025 cm^{-1}, was calculated between wave numbers of 2850 and 3000 cm^{-1}; see Fig. 4a. The integral area is proportional to the concentration of iC4 within the crystal. Plotting the time evolution of the normalized band intensity gives the uptake curve; a typical example is given in Fig. 4b. The continuous solid line in Fig. 4b is the fits using the analytical solution to Fick's second law for cylindrical crystal geometry $A_{norm} \equiv (A_t - A_0)/(A_\infty - A_0) = 1 - 4\sum_{n=1}^{\infty} 1/a_n^2 \exp\left(-a_n^2 Dt/r_{cyl}^2\right)$ where a_n are the roots of the zero-order Bessel function of the first kind $J_0(a_n) = 0$. The fits allow determination of the Fick diffusivity D for the chosen loading range. Due to the small loading steps employed in the uptake experiments the condition of a constant diffusivity implicit in the analytic solution is essentially fulfilled. As explained in detail in the Supplementary material, due to the geometry of the crystal used, the measured diffusivities reflect transport predominantly along the zig–zag channels, in the x-direction.

3. Results and discussion

The uptake kinetics of iC4 was measured for 25 differential loading steps. The gas phase pressure was varied from 0 to 0.1 MPa, corresponding to $0 < \Theta < 8.4$. The fitted values of the Fick diffusivity D are plotted in Fig. 5a as a function of the average loading Θ between the start and end of each uptake experiment. In Fig. 5a we detect two distinct 'regimes' in the loading dependence of the Fick diffusivity D. For the range $0 < \Theta < 4$, the D is practically constant, and independent of loading. In the range $4 < \Theta < 8.4$, the D increases sharply, by more than one order of magnitude with increasing Θ. The corresponding M–S diffusivity, $Đ$, backed out using $Đ = D/\Gamma$ is shown in Fig. 5b. As anticipated in earlier work [4–7] the measured data show a pronounced, cusp-like, inflection at $\Theta = 4$.

In order to obtain further insights into $Đ$–Θ behavior, we also performed KMC simulations [6,18–20]; see Supplementary material for simulation details. Let ν_{str} and ν_{zz} denote the jump frequencies along the straight and zig–zag channels when moving towards the intersections. There is evidence to suggest that the jump frequencies along the straight channels are greater than along the zig–zag channels $\nu_{str} > \nu_{zz}$ [20–22]. For iC4, the jumps away from the intersections towards either the straight or zig–zag channels occur at a frequency, lower by a factor f, because of the preference of iC4 to locate in the channel intersections. This factor f is determined by the ratio of the Langmuir constants in the DSL fit: $f = b_B/b_A = 0.0000285/0.024 = 0.0012$; the arguments behind the choice of f are given in earlier publications [6,18]. The asymmetry in the jump frequencies towards and away from the intersections captures the inflection behavior of the adsorption isotherm. The jump frequencies towards the intersection sites along zig–zag channels, the predominant direction of transport in the IRM experiments, are chosen to be $2.0 \times 10^9\ s^{-1}$ in order to match the zero-loading value, $Đ(0) = 1.2 \times 10^{-12}\ m^2\ s^{-1}$. The jump frequency along the straight channels is assumed to have a higher value $\nu_{str} = 3.5 \times 10^9\ s^{-1}$, but the precise value of this frequency has a negligible impact on the results and also on the conclusions of this work, because we only report the diffusivities in the x-direction (i.e. along the zig–zag channels) for comparison with IRM data. Furthermore, drawing inspiration from the work of Reed and Ehrlich [23], we

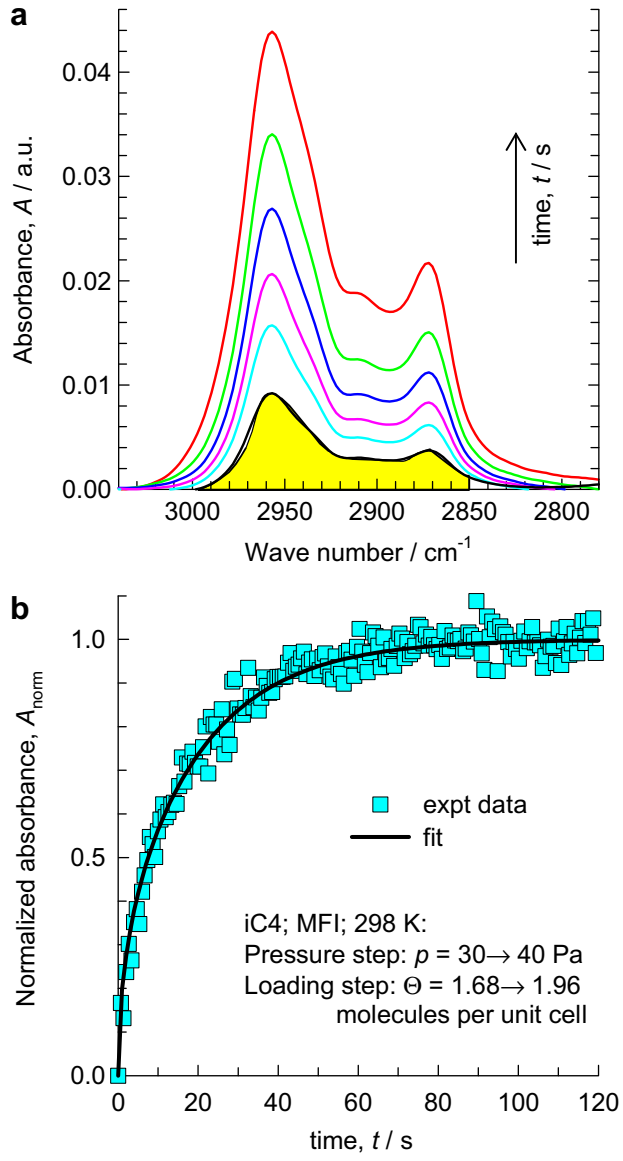

Fig. 4. (a) Absorption spectra recorded with time progression. The area under the band between wave numbers of 2850 and 3000 cm^{-1} is proportional to concentration of iC4 within the crystal. (b) Example of normalized uptake data along with the fitted curve.

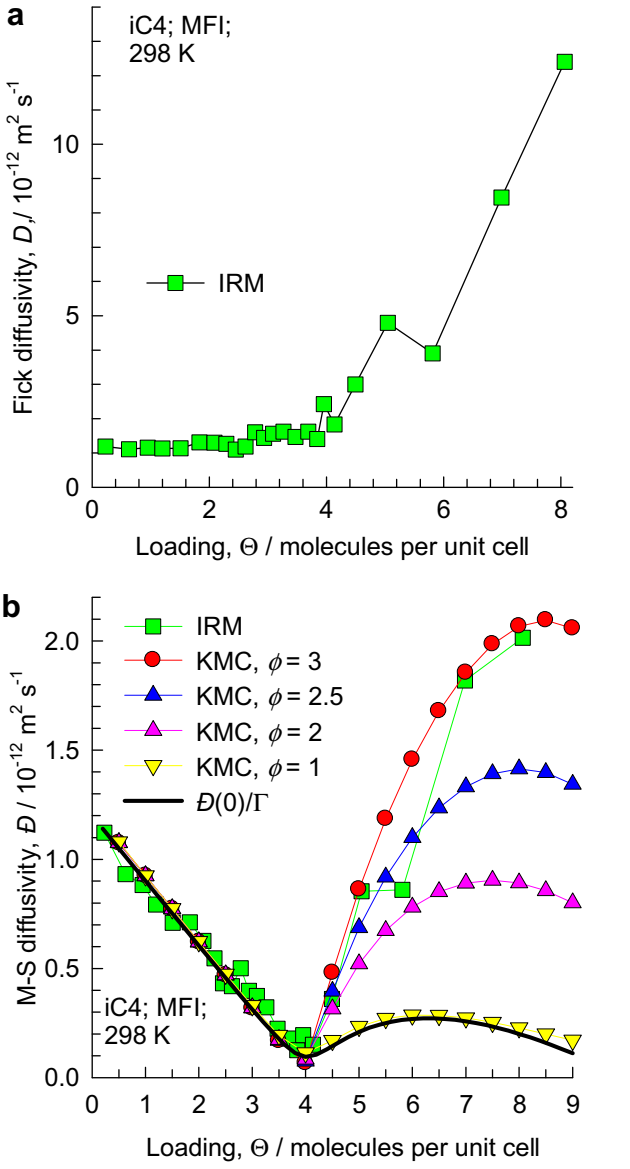

Fig. 5. (a) Fick diffusivity D as function of the loading in MFI. (b) Comparison of M–S diffusivity $Đ$ obtained from IRM experiments with KMC simulations with repulsion factors φ = 1, 2, 2.5, and 3.

have also allowed for repulsive interactions between the hopping molecules in our KMC scheme [18,24] by altering, i.e. increasing, the jump frequencies of molecule at any location by a factor φ for each molecule that occupies a neighbouring site. Comparison of the $Đ$ obtained from IRM experiments with KMC simulations with repulsion factors φ = 1 (no repulsions), 2, 2.5, and 3 are shown in Fig. 5b. The result for φ = 1, i.e. the situation with no repulsions, coincides very closely with the simple model $Đ = Đ(0)/\Gamma$ that was proposed in earlier work [4]. Even though this simple model is able to portray inflection characteristics, it severely underestimates the $Đ$ values for $\Theta > 4$. The IRM data are best reproduced taking φ = 3, suggesting strong inter-molecular repulsions are in play for $\Theta > 4$ when iC4 occupies channel locations (cf. Fig. 2b) and the proximity between molecules is closer than for $\Theta < 4$. Repulsive interactions that manifest at $\Theta > 4$ also cause the activation energy for diffusion to be lower than that for $\Theta > 4$; there is experimental data for diffusion of iC4 and 3-methylpentane in MFI to support this contention [1,20].

4. Conclusions

IRM experiments have been performed to determine the M–S diffusivity $Đ$ in MFI zeolite for a range of loadings $0 < \Theta < 8.4$ molecules per unit cell. These experiments indicate a strong inflection in $Đ$ vs. Θ at $\Theta = 4$. The data in Fig. 5 provide experimental confirmation of the inflection behavior that was anticipated by KMC and MD simulations [4–7]. The experimental data is quantitatively matched by KMC simulations provided inter-molecular repulsions are taken into consideration.

On the basis of the experimental data presented here, we may expect similar strong inflection behavior in $Đ$ vs. Θ for other branched alkanes, and aromatics (e.g. benzene, ethylbenzene). This inflection behavior has a strong influence on permeation fluxes across an MFI membrane [25].

Acknowledgements

Financial support by *Deutsche Forschungsgemeinschaft* (Mercator Professorship for RK, International Research Group 'Diffusion in

Zeolites' and International Research Training Group 'Diffusion in Porous Materials'), *Max-Buchner-Forschungsstiftung* and *Fonds der Chemischen Industrie* is gratefully acknowledged.

Appendix A. Supplementary data

Supplementary data associated with this article can be found, in the online version, at doi:10.1016/j.cplett.2008.05.023.

References

[1] R. Krishna, R. Baur, Sep. Purif. Technol. 33 (2003) 213.
[2] R. Baur, R. Krishna, Chem. Eng. J. 99 (2004) 105.
[3] R. Baur, R. Krishna, Catal. Today 105 (2005) 173.
[4] R. Krishna, J.M. van Baten, Chem. Phys. Lett. 420 (2006) 545.
[5] R. Krishna, J.M. van Baten, Chem. Phys. Lett. 407 (2005) 159.
[6] R. Krishna, J.M. van Baten, D. Dubbeldam, J. Phys. Chem. B 108 (2004) 14820.
[7] R. Krishna, J.M. van Baten, Micropor. Mesopor. Mater. 109 (2008) 91.
[8] H. Jobic, C. Laloué, C. Laroche, J.M. van Baten, R. Krishna, J. Phys. Chem. B 110 (2006) 2195.
[9] S. Li, J.L. Falconer, R.D. Noble, R. Krishna, J. Phys. Chem. C 111 (2007) 5075.
[10] R. Krishna, J.M. van Baten, E. García-Pérez, S. Calero, Ind. Eng. Chem. Res. 46 (2007) 2974.
[11] W. Zhu, F. Kapteijn, J.A. Moulijn, Phys. Chem. Chem. Phys. 2 (2000) 1989.
[12] T.J.H. Vlugt, W. Zhu, F. Kapteijn, J.A. Moulijn, B. Smit, R. Krishna, J. Am. Chem. Soc. 120 (1998) 5599.
[13] T.J.H. Vlugt, R. Krishna, B. Smit, J. Phys. Chem. B 103 (1999) 1102.
[14] M. Schenk, S.L. Vidal, T.J.H. Vlugt, B. Smit, R. Krishna, Langmuir 17 (2001) 1558.
[15] R. Krishna, B. Smit, S. Calero, Chem. Soc. Rev. 31 (2002) 185.
[16] W. Zhu, A. Malekian, M. Eic, F. Kapteijn, J.A. Moulijn, Chem. Eng. Sci. 59 (2004) 3827.
[17] C. Chmelik, et al., Chem. Mater. 19 (2007) 6012.
[18] R. Krishna, J.M. van Baten, Chem. Eng. Technol. 28 (2005) 160.
[19] R. Krishna, D. Paschek, Chem. Eng. J. 85 (2002) 7.
[20] D. Paschek, R. Krishna, Chem. Phys. Lett. 342 (2001) 148.
[21] D. Paschek, R. Krishna, Langmuir 17 (2001) 247.
[22] D. Paschek, R. Krishna, Phys. Chem. Chem. Phys. 2 (2000) 2389.
[23] D.A. Reed, G. Ehrlich, Surf. Sci. 102 (1981) 588.
[24] R. Krishna, D. Paschek, R. Baur, Micropor. Mesopor. Mater. 76 (2004) 233.
[25] R. Krishna, T.J.H. Vlugt, B. Smit, Chem. Eng. Sci. 54 (1999) 1751.

Supplementary Material to accompany:

Inflection in the loading dependence of the Maxwell-Stefan diffusivity of *iso*-butane in MFI zeolite

C. Chmelik[(1)], L. Heinke [(1)], J. Kärger[(1)], W. Schmidt[(2)], D.B. Shah[(3)], J.M. van Baten[(4)] and R. Krishna[(4)]*

[(1)] Abteilung Grenzflächenphysik, Universität Leipzig, Linnéstraße 5, 04103 Leipzig, Germany

[(2)] Max Planck Institute for Coal Science, Kaiser-Wilhelm-Platz 1, D-45470 Mülheim, Germany

[(3)] Department of Chemical & Biomedical Engineering, Cleveland State University, 2121 Euclid Avenue, Cleveland, Ohio 44115 USA

[(4)] Van 't Hoff Institute for Molecular Sciences, University of Amsterdam, Nieuwe Achtergracht 166, 1018 WV Amsterdam, The Netherlands

Appendix A1: Experimental set-up, experimental procedure, diffusivity determinations

1. Experimental Method

The results discussed in the main part were obtained using the IR microscope HYPERION 3000 coupled with an IR spectrometer VERTEX 80v (both *Bruker Optics*). The schematic diagram of the IR microscopy (IRM) measurement set-up is shown in Figure 1.

At first, several hundred crystals were introduced into the IR cell and activated as described later in this document. Then, in the viewing mode of the microscope, one particular zeolite crystal was selected by moving the motorized sample platform and adopting the aperture accordingly (see Figure 1). The rectangular aperture selects the region in the field of view which is scanned by IR light. Here, the size was set to about $100 \times 220\ \mu m^2$. All measurements were preformed in the IR-transmittance mode of the microscope. Prior to the uptake experiments, the crystal was checked for anomalies in the IR spectrum, e.g. present C-H or water bands, to exclude a non-proper activation.

For controlling the gas phase composition in the IR cell, it is attached to a static vacuum system, consisting of turbo-molecular pump, pressure transducers, stock volume and gas bottle with the sorbate. The adsorption or desorption steps were initiated by step changes in the gas phase surrounding the crystals. All experiments were carried out at room temperature, i.e. at 298 K.

To follow the uptake or release of the *iso*-butane (iC4) within the crystal, absorption spectra were recorded with a temporal resolution between 0.2 – 1.5 s. The spectral resolution was set to 16 cm^{-1}. The area under the C-H stretching band, enclosed by a straight baseline between 2800 and 3025 cm^{-1}, was calculated between 2850 and 3000 cm^{-1} (see Figure 2 of the paper). No further transformations or corrections of the spectra were required. Following the Beer-Lambert law $A = \log\left(I_0 / I\right) = \alpha_{\mathrm{m}} \cdot c \cdot d$

the integrals were assumed to be proportional to the concentration c of the iC4 guest molecules in the crystal. Here, A denotes the absorbance, I and I_0 are the intensities of the sample scan and background scan, respectively, α_m is the coefficient of molar extinction and d is the thickness of the medium.

Plotting the time evolution of the normalized band intensity gives the integral uptake curve which can be analysed by an appropriate solution of Fick's second law to calculate the transport diffusivity [1-3].

2. Samples

Silicalite-1 belongs to zeolites with MFI type structure. These crystalline aluminosilicates consist of AlO_4^- and SiO_4 tetrahedra linked by oxygen bridges to form 5-1 secondary building units [4,5]. Silicalite-1 is defined to have a Si/Al ratio of larger than 1000. The building units form a three-dimensional pore system of straight channels in y-direction [010], which are cross-linked by sinusoidal channels in x-direction [100] (see Figure 3). By an alternating use of the straight and sinusoidal channels mass transport can proceed also along the z-direction [001]. The cross-sections are given with $5.3\times5.6\,\text{Å}^2$ and $5.1\times5.5\,\text{Å}^2$ for the straight and sinusoidal channels, respectively [4]. Measured from one intersection centre to the next, the straight segments have a length of 9.95 Å, whereas the zig-zag segments have a length of 12.07 Å. The unit cell parameters are a = 20.07 Å, b = 19.74 Å and c = 13.14 Å [4].

The silicalite-1 crystals used for this study were synthesized at the Max-Planck-Institute in Mülheim, Germany and provided in calcined form. Further details of the synthesis can be found in [6]. The investigated crystals were approximately $25\times25\times180\ \mu m^3$ in size. The crystals exhibit an internal intergrowth structure, caused by a twinning with of the individual single-crystal segments. The orthogonal arrangement of the segments involves that the crystallographic axis of two segments is rotated by 90° around the z-axis (see Figure 3).

As a consequence of the intergrowth, the openings of the straight channels lead only to the internal interfaces and only the sinusoidal channels have access to the outer surface of the prism segments.

Hence, the uptake in these crystals will be dominated by transport along the zig-zag channels. In contrast to our previous study [7], in more recent work no influence of the internal intergrowth faces on molecular transport of *iso*-butane could be observed for silicalite-1 crystals from the same batch investigated here [8].

For activation, several hundred crystals were introduced in the IR cell and heated under vacuum ($<10^{-5}$ mbar) with a heating rate of 1 K·min^{-1}. Then, the crystals were kept at a temperature of 753 K for 24 h. In addition, a calcination step under presence of oxygen was attached for about 2 h, to remove possibly existing coked organic residuals. Subsequently, the crystals were again exposed to vacuum for 3 h. After cooling the crystals to room temperature the sorption experiments were started.

3. Determination of Fick diffusivity

For each adsorption step the uptake curves were normalized to go from 0 at t = 0 to unity at equilibrium. To calculate the transport diffusivity the solution of Fick's second law for uptake in infinitely long extended, cylindrical shaped particles with three-dimensional pore network [1] was fitted to the experimental data,

$$A_{norm} \equiv \frac{A_t - A_0}{A_\infty - A_0} = 1 - 4\sum_{n=1}^{\infty} \frac{1}{a_n^2} \exp\left(-\frac{a_n^2 D t}{r_{cyl}^2}\right) \qquad (1)$$

where a_n are the roots of the zero-order Bessel function $J_0(a_n) = 0$. r_{cyl} the equivalent cylinder radius calculated as $r_{cyl} = w \cdot h/(w+h)$ with w and h representing the crystal extension along x' and y'-direction (both approximately 25 µm). A_0, A_t, and A_∞ denote the absorbance at time 0, t and ∞, respectively. Hence, the normalized absorbance A_{norm} reflects the fractional uptake at time t. In the fits the sum was calculated up to the 100th term. Due to the outer shape of the investigated crystals, the 90°-intergrowth and small diffusivity along z-direction, this solution of Fick's second law represents a reasonable approximation for the uptake in the given system.

Diffusion Anisotropy

Molecular simulations suggest differences in the *iso*-butane diffusivity along the different crystallographic directions [3,9,10]. As discussed in the previous section, the uptake in crystals will be dominated by transport along the zig-zag channels. A more detailed consideration reveals that the straight channels in the two pyramidal parts contribute somewhat to the overall uptake. Based on the volume ratio of the pyramidal parts to the four large prisms of about 1:4 one can estimate the contribution of flux occurring along the straight channels to about 10-15%. Due to the aspect ratio, i.e. long and thin shape of the crystals, the contribution of transport along the *z*-axis can be neglected in analysis of the IR measurements.

In summary, the particular orientation of the crystal segments and the specific diffusion anisotropy of iso-butane in MFI-type zeolites implies that the uptake in our MFI crystals will be dominated by transport along the zig-zag channels.

4. Experimental Data

Equilibrium Isotherm

For a proper interpretation of the concentration dependence the knowledge of the adsorption isotherm is essential. Therefore, single crystal sorption isotherms were recorded for three different, individual crystals. The gas phase pressure of *iso*-butane was increased in small steps between vacuum and 20 mbar [11]. For each step the absorbance was measured at equilibrium. The results were plotted against pressure (see Figure 4). Small differences in the size of crystals originally produced small deviations between the values of integral concentration. To compensate the influence of the size differences the isotherms of crystal 2 and 3 were scaled to follow the data of crystal 1. After this procedure all isotherms showed perfect agreement. To determine the absolute concentration the IR data were compared with the results of CBMC simulations. Both isotherms are in excellent agreement in the considered range. Therefore, the dual-site Langmuir fit obtained from the CBMC data was used to calculate the equilibrium concentration in the IR experiments.

Uptake Measurements

The uptake kinetics of *iso*-butane in silicalite-1 was measured for about 25 differential loading steps. The gas phase pressure was varied from 0 to 0.1 MPa, corresponding to an intracrystalline loading between 0 and 8.4 molecules per unit cell. Due to the small loading steps covered in the uptake experiments the condition of a constant diffusivity implied in Eq. (1) is practically fulfilled. Four typical examples, showing the good agreement between experimental data and the fits are plotted in Figure 5.

.

5. References

[1] J. Crank, *Mathematics of Diffusion*, Oxford University Press, 2nd Edition, 1975.

[2] H.G. Karge and W. Niessen; *Catal. Today* **8** (1991) 451-465.

[3] J. Kärger and D.M. Ruthven, *Diffusion in Zeolites and Other Microporous Solids*; Wiley & Sons, New York, 1992.

[4] Ch. Baerlocher and L.B. McCusker, Database of Zeolite Structures: http://www.iza-structure.org/databases/ .

[5] Ch. Baerlocher, W.M. Meier and D.H. Olson, *Atlas of Zeolite Framework Types*; 5th revised edition, Elsevier, Amsterdam, 2001.

[6] W. Schmidt, U. Wilczok, C. Weidenthaler, O. Medenbach, R. Goddard, G. Buth and A. Cepak; *J. Phys. Chem. B* **111** (2007) 13538-13543.

[7] O. Geier, S. Vasenkov, E. Lehmann, J. Kärger, U. Schemmert, R.A. Rakoczy and J. Weitkamp; *J. Phys. Chem. B* **105** (2001) 10217-10222.

[8] D. Tzoulaki, L. Heinke, W. Schmidt, U. Wilczok and J. Kärger; Exploring Crystal Morphology of Nanoporous Hosts from Transient Guest Profiles, *Angew. Chem.* (2008) accepted.

[9] A. Bouyermaouen and A. Bellemans; *J. Chem. Phys.* **108** (1998) 2170-2172.

[10] T.J.H. Vlugt, C. Dellago, B. Smit; *J. Chem. Phys.* **113** (2000) 8791-8799.

[11] C. Chmelik, A. Varma, L. Heinke, D.B. Shah, J. Kärger, F. Kremer, U. Wilczok and W. Schmidt; *Chem. Mater.* **19** (2007) 6012-6019.

6. Captions for Figures

Figure 1. Photograph of the Infra-Red microscopy (IRM) experimental set-up. The upper-right picture depicts the crystal observed with the microscope set in the viewing model. The bottom-right picture is a close-up of the motorized platform on which the crystal is placed.

Figure 2. Absorption spectra recorded with time progression. The area under the band between wave numbers of 2850 and 3000 cm^{-1} is proportional to concentration of iC4 within the crystal.

Figure 3. Schematic representation of the internal structure of the investigated MFI crystals and the channel network. The orientation of the crystal segments was taken from [6].

Figure 4. Isotherm data obtained from IRM for crystals 1, 2 and 3 at 298 K. The continuous solid line represents the DSL fit of CBMC simulations (data reported in Appendix A2).

Figure 5. Comparison of normalized uptake curves determined by IR microscopy with best fits using Eq. (1) for four different loading steps. In the legend to abbreviation muc stands for molecules per unit cell.

Figure 1

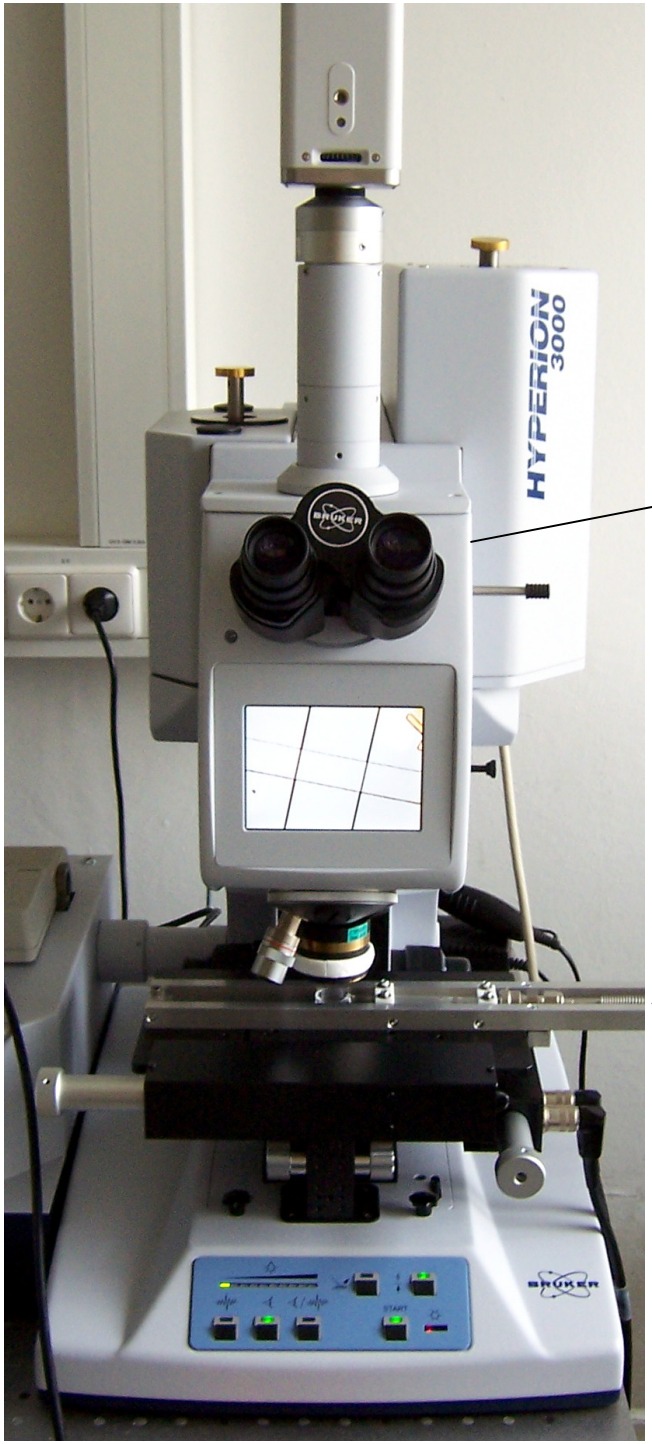

Viewing mode of microscope for adjusting the aperture

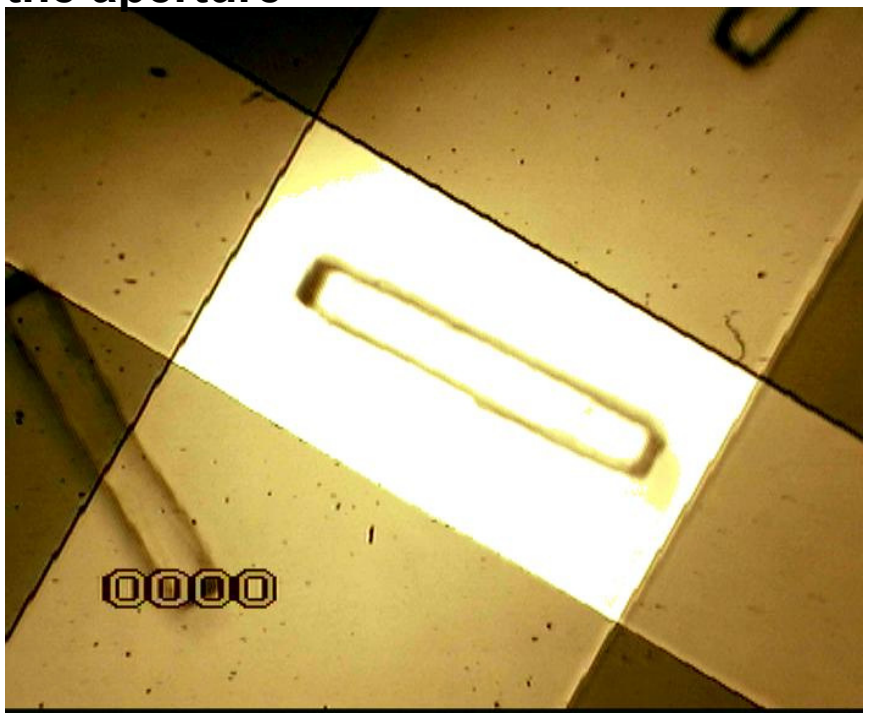

crystal mounted on moving platform

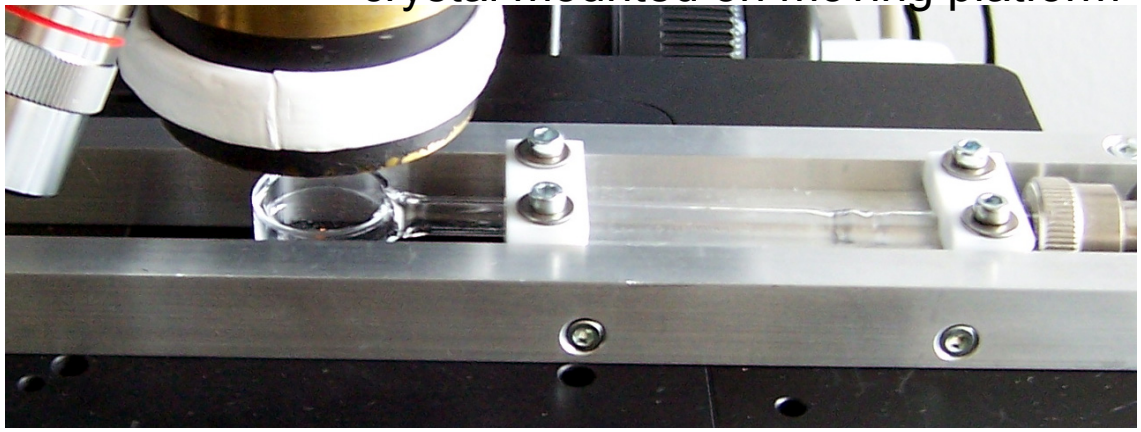

Figure 2

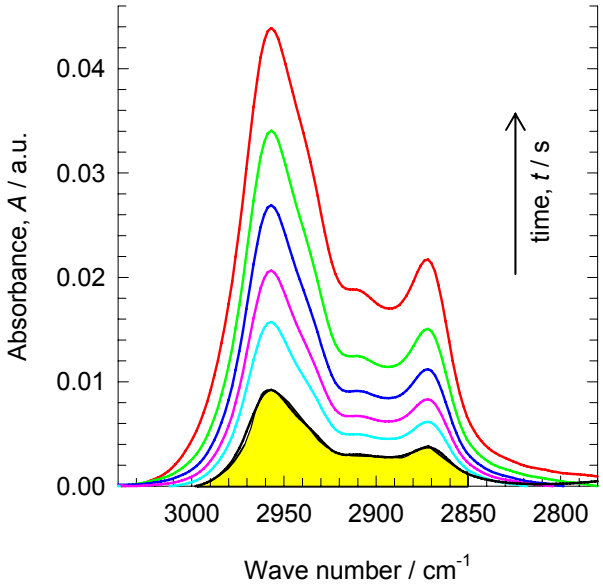
0.04
0.03
0.02
0.01
0.00
Absorbance, A / a.u.
3000
2950
2900
2850
2800
Wave number / cm-1
time, t / s

Figure 3

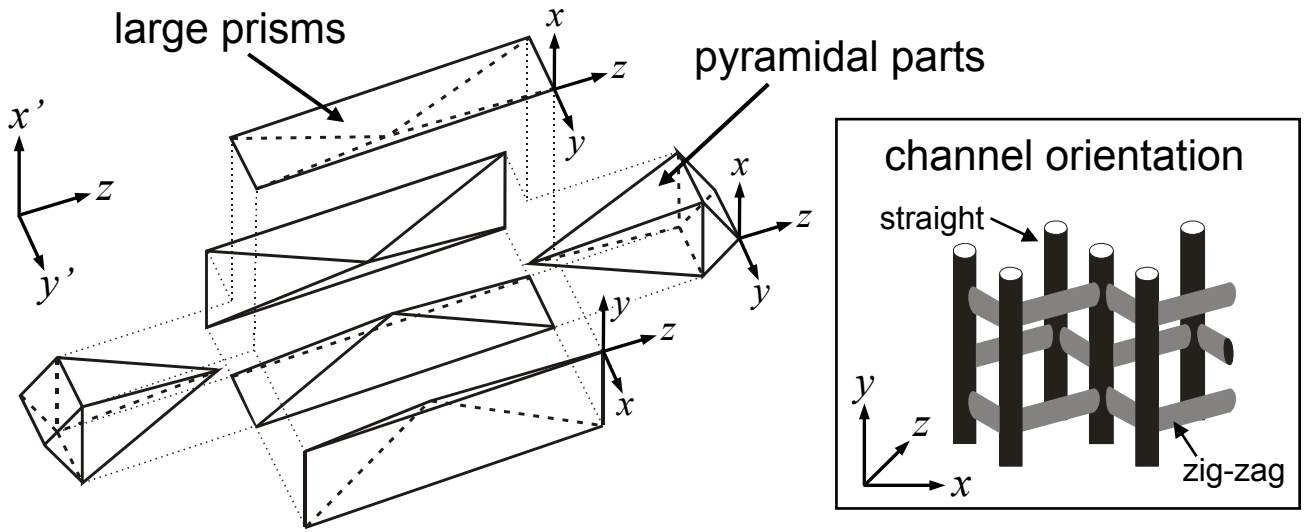
large prisms
pyramidal parts
x
z
y
x'
z
y'
x
z
y
y
z
x
channel orientation
straight
y
z
x
zig-zag

Figure 4

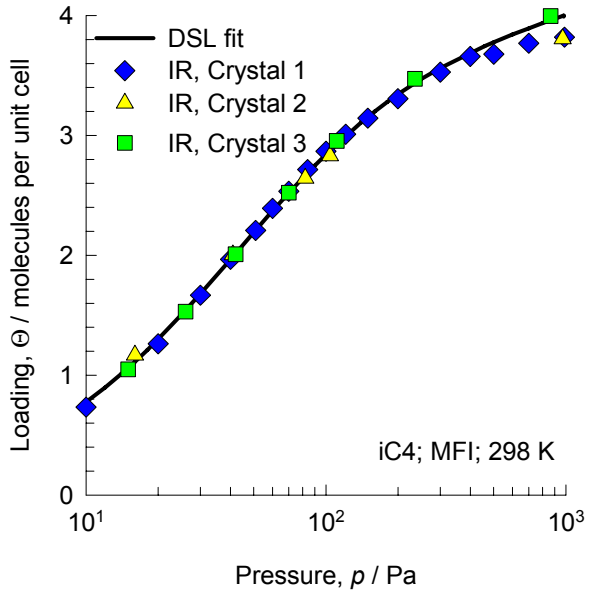
DSL fit
IR, Crystal 1
IR, Crystal 2
IR, Crystal 3
iC4; MFI; 298 K
Loading, Θ / molecules per unit cell
Pressure, p / Pa
0
1
2
3
4
10^1
10^2
10^3

Figure 5

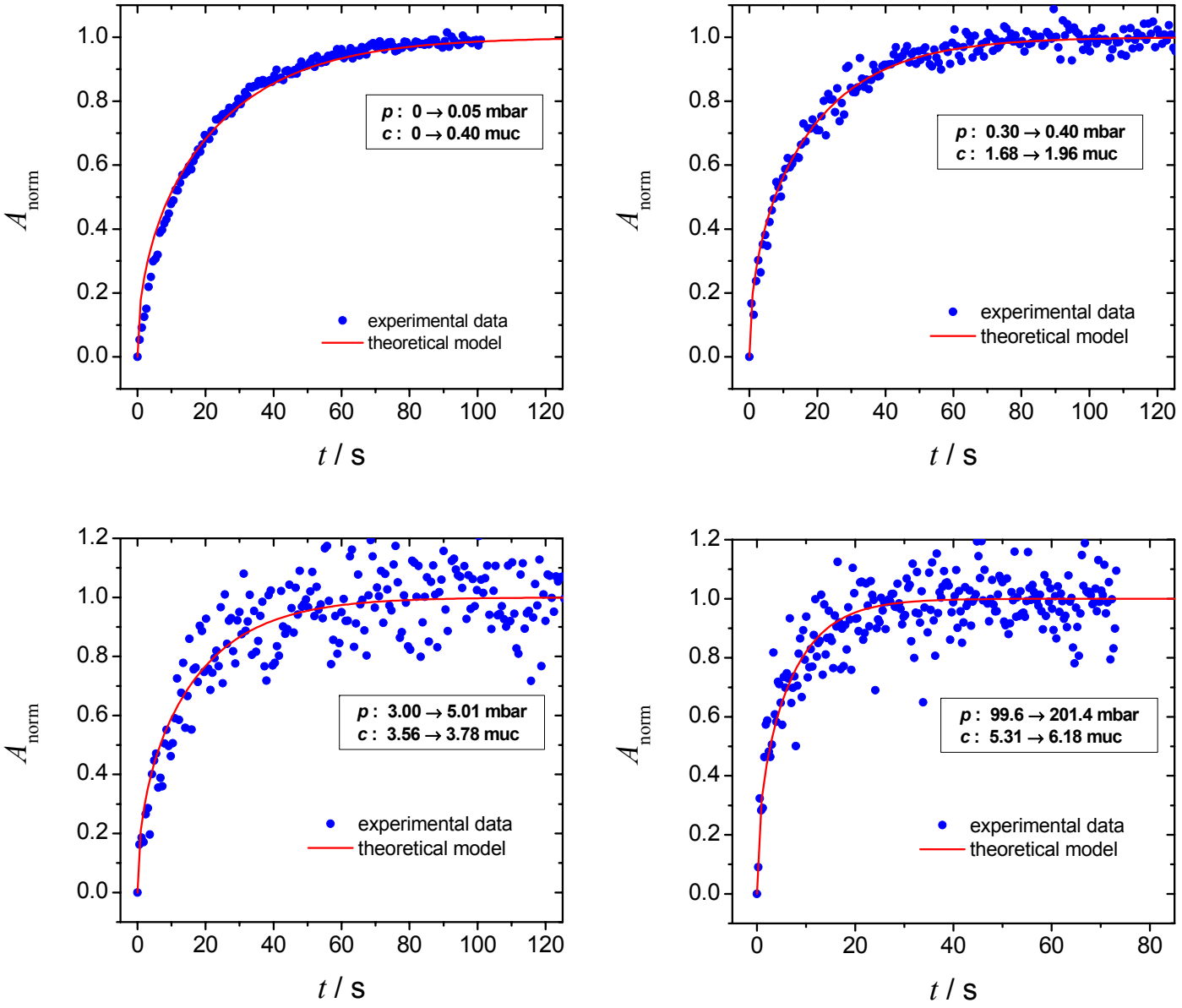
A_{norm}
t / s
p : 0 → 0.05 mbar
c : 0 → 0.40 muc
experimental data
theoretical model
p : 0.30 → 0.40 mbar
c : 1.68 → 1.96 muc
p : 3.00 → 5.01 mbar
c : 3.56 → 3.78 muc
p : 99.6 → 201.4 mbar
c : 5.31 → 6.18 muc

Appendix A2: Simulation methodology and results

1. CBMC simulations

Configurational-Bias Monte Carlo (CBMC) simulations have been carried out to determine the adsorption isotherms for iC4 in MFI (all silica silicalite-1) at 298 K; the crystallographic data are available elsewhere[1, 2]. We use the united atom model. The zeolite framework is considered to be rigid. We consider the CH_x groups as single, chargeless interaction centers with their own effective potentials. The beads in the chain are connected by harmonic bonding potentials. A harmonic cosine bending potential models the bond bending between three neighboring beads, a Ryckaert-Bellemans potential controls the torsion angle. The beads in a chain separated by more than three bonds interact with each other through a Lennard-Jones potential. The Lennard-Jones potentials are shifted and cut at 12 Å. The CBMC simulation details, along with the force fields have been given in detail in earlier publications[3, 4]. The simulation box consists of 2×2×4 unit cells for MFI. Periodic boundary conditions were employed. It was verified that the size of the simulation box was large enough to yield reliable data on adsorption.

The CBMC simulations were performed using the BIGMAC code developed by T.J.H. Vlugt[5] as basis. The code was modified to handle rigid molecular structures and charges. S. Calero is gratefully acknowledged for her technical inputs in this regard.

Snapshots of the location of iC4 molecules at loadings of 2, 4 and 6 molecules per unit cell are shown in Figures 1 and 2. We see that for loadings < 4, the iC4 is located predominantly at the intersections between the straight and zig-zag channels. For loading >4, iC4 can be made to locate within the channels.

Comparisons between experimental data of Sun et al.[6] and Zhu et al.[7] and CBMC simulation for the isotherms for iC4 in MFI at a variety of temperatures are given in Figure 3. The inflection in the

isotherm is accurately captured by the CBMC simulations. Indeed the force fields for alkanes were chosen to represent the isotherm inflection accurately[3, 4].

The continuous solid lines in Figures 4 are dual-site Langmuir fits of the isotherm

$$\Theta = \frac{\Theta_{sat,A} b_A p}{1 + b_A p} + \frac{\Theta_{sat,B} b_B p}{1 + b_B p} \qquad (1)$$

The values of the fitted parameters b and Θ_{sat} are specified in Table 1.

2. Kinetic Monte Carlo (KMC) Simulations

In order to rationalize the loading dependence of the M-S diffusivity for iC4 in MFI we performed Kinetic Monte Carlo (KMC) simulations following the methodology outlined in earlier publications [8-14]. The MFI lattice topology (see Fig. 5) is made up of equal sized sorption sites, 12 in total, distributed along the straight channels (4), zig-zag channels (4) and at the intersections (4). A total of 2×2×4 = 16 unit cells were simulated. In the KMC simulations we assume that the each site can be occupied by only one molecule at a time. Particles can move from one site to a neighboring site via hops. Let ν_{str} and ν_{zz} denote the jump frequencies along the straight and zig-zag channels when moving *towards* the intersections. Based on MD simulations it is concluded that the frequencies along the straight channels is greater than along the zig-zag channels $\nu_{str} > \nu_{zz}$ [8-10]. For iC4, the jumps *away* from the intersections towards either the straight or zig-zag channels occur at a frequency, lower by a factor f, because of the preference of iC4 to locate in the channel intersections. This factor f is determined by the ratio of the Langmuir constants in the DSL fit: $f = b_B / b_A = 0.0000285 / 0.025 = 0.0012$; the arguments behind the choice of f are given in earlier publications[11, 12]. The asymmetry in the jump frequencies towards and away from the intersections captures the inflection behavior of the sorption isotherm. In the IRM experiments the transport along the zig-zig channels dominates the uptake process (See discussions in Appendix A1), and it is the diffusivity along the x-direction that is of primary interest. The jump frequency along the zig-zag channels was chosen to match the value of the zero-loading Maxwell-Stefan diffusivity of iC4 as

obtained in the IRM experiments, i.e. $D(0) = 1.2\times10^{-12}$ m^2 s^{-1}; this gives $\nu_{zz} = 2\times10^9$ s^{-1}. The jump frequency along the straight channels is assumed to have a higher value $\nu_{str} = 3.5\times10^9$ s^{-1}, but the precise value of this frequency has a negligible impact on the results and on the conclusions of this work, because we only report the diffusivities in the x-direction for comparison with IRM data.

We employ a standard KMC methodology to propagate the system [8, 9, 15-18]. A hop is made every KMC step and the system clock is updated with variable time steps. For a given configuration of random walkers on the lattice a process list containing all possible M moves to vacant intersection sites is created. Each possible move i is associated with a jump probability ν_i. Note that the values depend on the particular type a particle belongs to, as well as on the possible occupation of neighbouring sites. The *mean* elapsed time τ is the inverse of the total rate coefficient

$$\tau^{-1} = \nu_{total} = \sum_{i=1}^{M} \nu_i \qquad (2)$$

which is then determined as the sum over all processes contained in the process list. The actual KMC time step Δt for a given configuration is randomly chosen from a Poisson distribution

$$\Delta t = -\ln(u)/\nu_{total} \qquad (3)$$

where $u \in [0,1]$ is a uniform random deviate. The time step Δt is independent from the chosen hopping process. To select the actual jump, we define process probabilities according to $p_i = \sum_{j=1}^{i} \nu_j / \nu_{total}$. The ith process is chosen, when $p_{i-1} < \upsilon < p_i$, where $\upsilon \in [0,1]$ is another uniform random deviate. After having performed a hop, the process list is updated. In order to avoid wall effects we employ periodic boundary conditions.

In order to account for nearest neighbour interactions, the transition rates have to be altered if another particle occupies an adjacent site. The employed procedure is illustrated in Fig. 6. It is based on the assumption that the logarithm of the hopping rate is proportional to the relative height of the energy barrier, as for example given by $E_{trans} - E_A$ for the move from A to B. Consider two neighboring

particles at positions A and B. In order to ensure energy conservation, both particles have to experience the same repulsive interaction δE_{AB}. The depth of the potential well of a particle at position A is modified by δE_A, which is determined by summing over all possible nearest-neighbor interactions

$$\delta E_A = \sum_B \delta E_{AB} \tag{4}$$

Here B indicates all *occupied* nearest neighbor positions with respect to A. In the KMC scheme the rates of all possible moves of the particle located at A have to be changed by a factor

$$\nu'_{A\to B'} = \nu_{A\to B'} \exp(\frac{\delta E_A}{RT}) \tag{5}$$

Here B' denotes all empty nearest neighbour positions with respect to A. Since we do not wish to introduce an explicit value for the temperature T here, the Arrhenius term in eq. (5) is replaced by a product of pair-pair interaction factors ϕ_{AB}

$$\nu'_{A\to B'} = \nu_{A\to B'} \prod_B \phi_{AB} \tag{6}$$

With

$$\phi_{AB} = \phi = \exp(\frac{\delta E_{AB}}{RT}) \tag{7}$$

Since only nearest neighbour interactions are involved, the scheme is simple and the computational effort is moderate. In our KMC simulations we study the influence of the pair-pair interaction factors ϕ set equal to 1 (no repulsions), or > 1 (finite repulsion). The value of ϕ can be chosen to match experimental data.

From the KMC simulations we calculate the M-S diffusivity $Đ$ from the mean square displacement of the centre of gravity of all n adsorbed particles in each of the coordinate directions:

$$Đ = \frac{1}{2}\lim_{\Delta t\to\infty}\frac{1}{\Delta t}\left\langle\left(\frac{1}{n}\sum_{i=1}^{n}\left(\mathbf{r}_i(t+\Delta t)-\mathbf{r}_i(t)\right)\right)^2\right\rangle \tag{8}$$

These diffusivities correspond to “corrected” diffusivities, as shown in the work of Reed and Ehrlich [19] and Tarasenko [20]. The choice of Δt has been discussed in previous publications [8, 9, 17, 18].

3. References

[1] C. Baerlocher, L.B. McCusker, Database of Zeolite Structures, International Zeolite Association, http://www.iza-structure.org/databases/, 26 June 2001.

[2] J.M. van Baten, R. Krishna, MD Simulations of Diffusion in Zeolites, University of Amsterdam, http://www.science.uva.nl/research/cr/md/,

[3] D. Dubbeldam, S. Calero, T.J.H. Vlugt, R. Krishna, T.L.M. Maesen, E. Beerdsen, B. Smit, Force Field Parametrization through Fitting on Inflection Points in Isotherms, Phys. Rev. Lett. 93 (2004) 088302.

[4] D. Dubbeldam, S. Calero, T.J.H. Vlugt, R. Krishna, T.L.M. Maesen, B. Smit, United Atom Forcefield for Alkanes in Nanoporous Materials, J. Phys. Chem. B 108 (2004) 12301-12313.

[5] T.J.H. Vlugt, BIGMAC, University of Amsterdam, http://molsim.chem.uva.nl/bigmac/, 1 November 2000.

[6] M.S. Sun, D.B. Shah, H.H. Xu, O. Talu, Adsorption equilibria of C_1 to C_4 alkanes, CO_2, and SF_6 on silicalite, J. Phys. Chem. B 102 (1998) 1466-1473.

[7] W. Zhu, F. Kapteijn, J.A. Moulijn, Adsorption of light alkanes on silicalite-1: Reconciliation of experimental data and molecular simulations, Phys. Chem. Chem. Phys. 2 (2000) 1989-1995.

[8] D. Paschek, R. Krishna, Monte Carlo simulations of self- and transport-diffusivities of 2-methylhexane in silicalite, Phys. Chem. Chem. Phys. 2 (2000) 2389-2394.

[9] D. Paschek, R. Krishna, Diffusion of binary mixtures in zeolites: Kinetic Monte Carlo versus molecular dynamics simulations, Langmuir 17 (2001) 247-254.

[10] D. Paschek, R. Krishna, Monte Carlo simulations of sorption and diffusion of isobutane in silicalite, Chem. Phys. Lett. 342 (2001) 148-154.

[11] R. Krishna, J.M. van Baten, D. Dubbeldam, On the Inflection in the Concentration Dependence of the Maxwell-Stefan diffusivity of CF_4 in MFI zeolite, J. Phys. Chem. B 108 (2004) 14820-14822.

[12] R. Krishna, J.M. van Baten, Kinetic Monte Carlo simulations of the loading dependence of diffusion in zeolites, Chem. Eng. Technol. 28 (2005) 160-167.

[13] R. Krishna, D. Paschek, Verification of the Maxwell-Stefan theory for tracer diffusion in zeolites, Chem. Eng. J. 85 (2002) 7-15.

[14] R. Krishna, D. Paschek, R. Baur, Modelling the occupancy dependence of diffusivities in zeolites, Microporous Mesoporous Mater. 76 (2004) 233-246.

[15] S.M. Auerbach, Theory and simulation of jump dynamics, diffusion and phase equilibrium in nanopores, Int. Rev. Phys. Chem. 19 (2000) 155-198.

[16] M.O. Coppens, A.T. Bell, A.K. Chakraborty, Dynamic Monte-Carlo and mean-field study of the effect of strong adsorption sites on self-diffusion in zeolites, Chem. Eng. Sci. 54 (1999) 3455-3463.

[17] D. Paschek, R. Krishna, Kinetic Monte Carlo simulations of transport diffusivities of binary mixtures in zeolites, Phys. Chem. Chem. Phys. 3 (2001) 3185-3191.

[18] D. Paschek, R. Krishna, Inter-relation between self- and jump-diffusivities in zeolites, Chem. Phys. Lett. 333 (2001) 278-284.

[19] D.A. Reed, G. Ehrlich, Surface diffusivity and the time correlation of concentration fluctuations, Surf. Sci. 105 (1981) 603-628.

[20] A.A. Tarasenko, L. Jastrabik, C. Uebing, Diffusion of interacting adsorbates on a square lattice, Langmuir 15 (1999) 5883-5892.

Table 1. Dual-site Langmuir parameters for iC4 in MFI at 298 K. The saturation capacity, q_{sat}, has the units of molecules per unit cell. The Langmuir parameters, b, have the units of Pa^{-1}.

b_A	$\Theta_{sat,A}$	b_B	$\Theta_{sat,B}$
2.4×10^{-2}	4	2.85×10^{-5}	6

4. Captions for Figures

Figure 1. Snapshots showing location of iC4 at loadings of 2, and 4 molecules per unit cell in MFI.

Figure 2. Snapshots showing location of iC4 at loading of 6 molecules per unit cell in MFI.

Figure 3. Comparison of GCMC simulations for pure component isotherms for iC4 in MFI with experimental data of Sun et al.[6] and Zhu et al.[7].

Figure 4. Pure component isotherm data for iC4 in MFI at 298 K. The filled symbols are CBMC simulation results. The continuous solid lines are dual-site Langmuir fits with parameters specified in Table 1.

Figure 5. KMC simulation strategy. The total number of adsorption sites is 12, distributed as shown.

Figure 6. Energy scheme used for KMC simulations used here. Two particles adsorbed at adjacent sites experience a repulsive interaction energy $\delta E_{\alpha\beta}$.

Figure 1

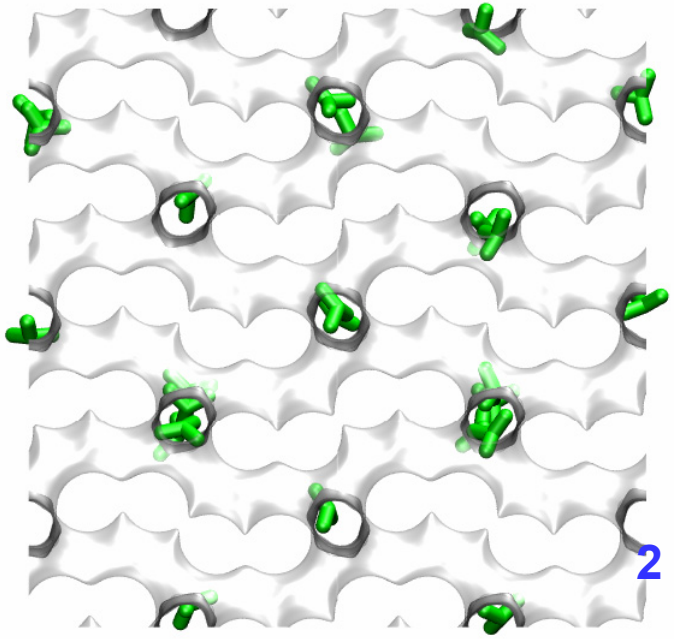

2 uc deep

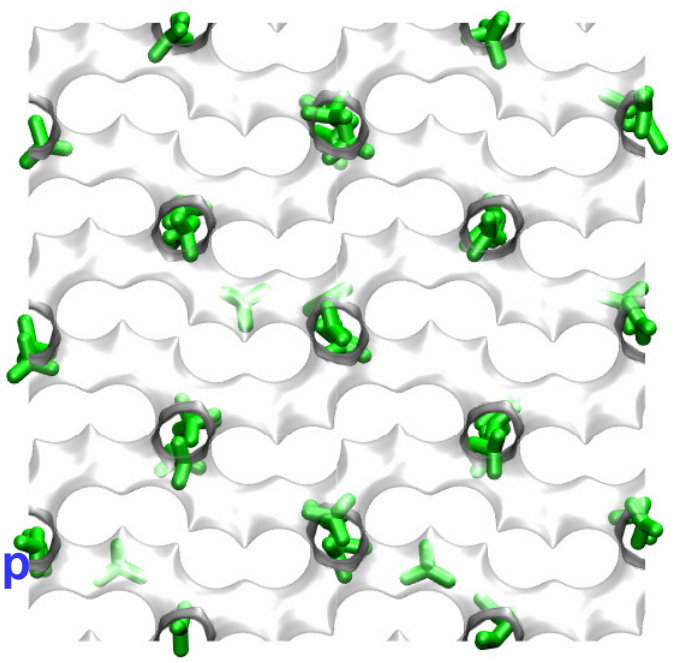

2 uc deep

iC4: 2 molecules/uc

iC4: 4 molecules/uc

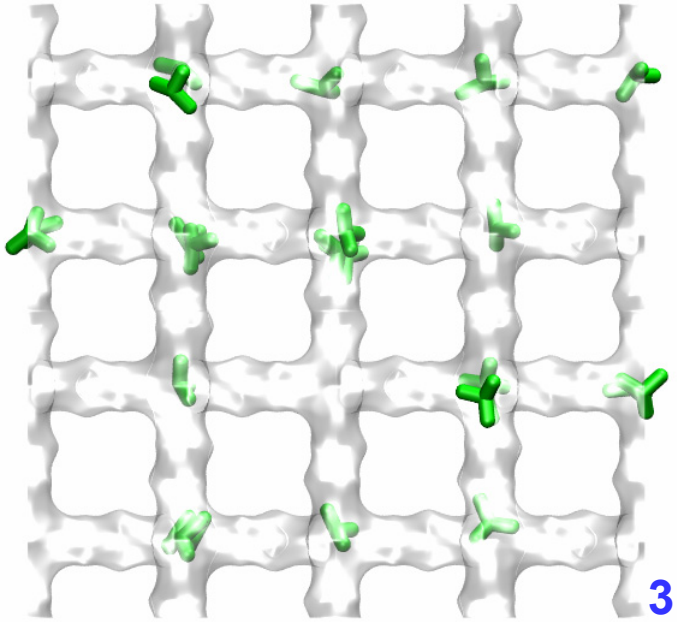

3 uc deep

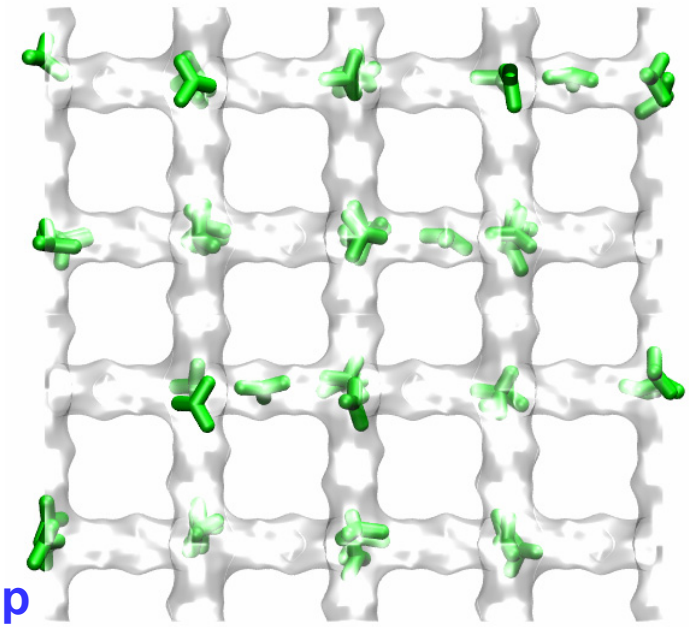

3 uc deep

Figure 2

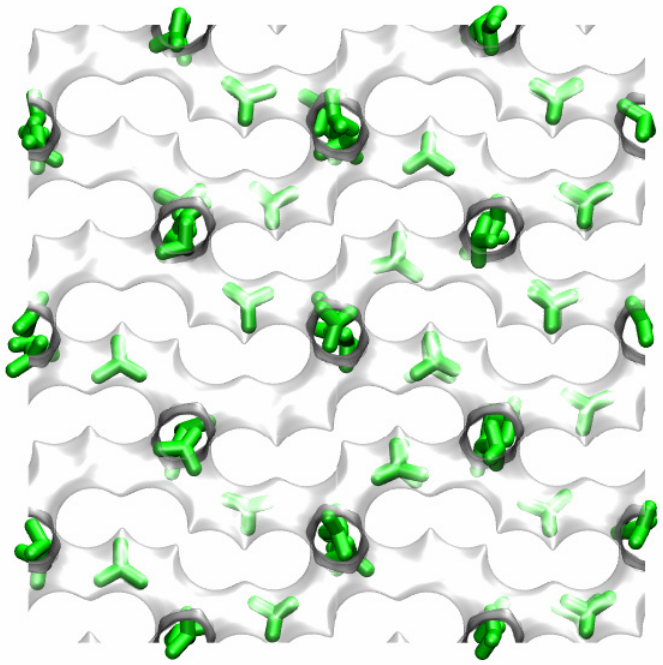

2 uc deep

iC4: 6 molecules/uc

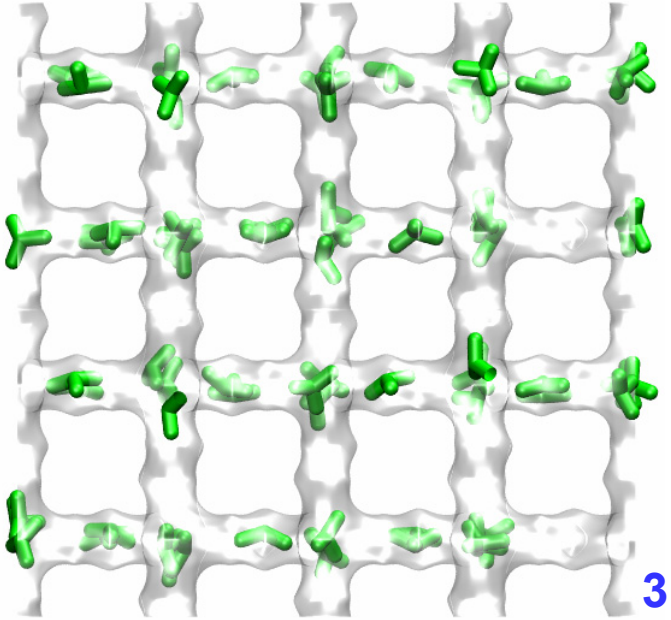

3 uc deep

Figure 3

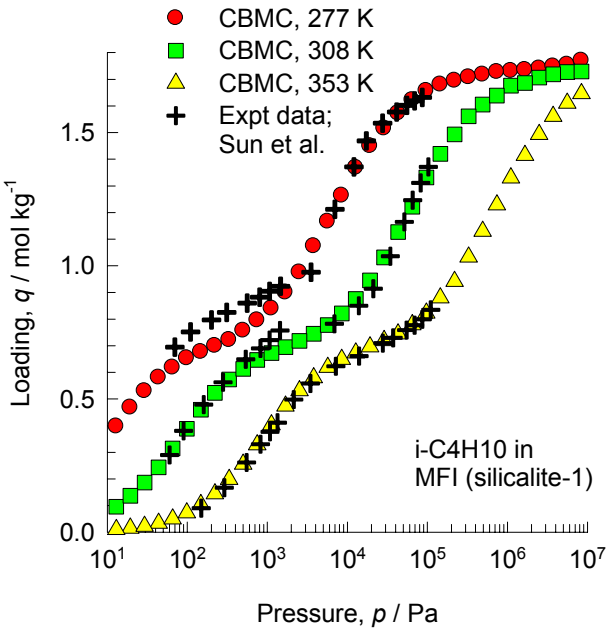
CBMC, 277 K
CBMC, 308 K
CBMC, 353 K
Expt data;
Sun et al.
i-C4H10 in
MFI (silicalite-1)
Loading, q / mol kg-1
Pressure, p / Pa
0.0
0.5
1.0
1.5
10^1
10^2
10^3
10^4
10^5
10^6
10^7

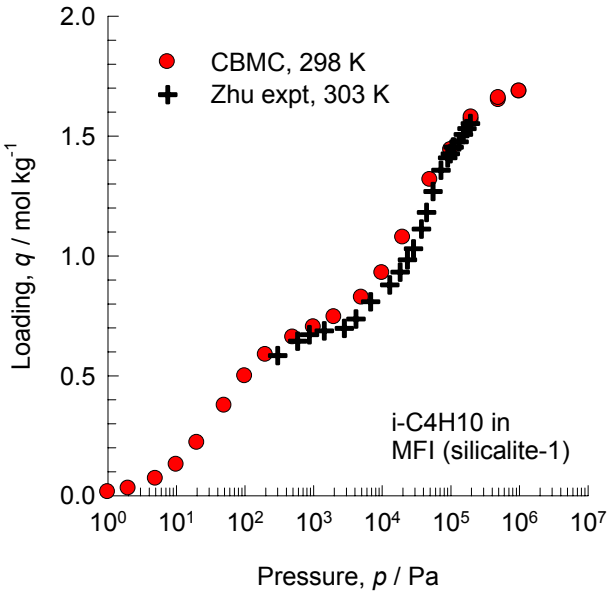
CBMC, 298 K
Zhu expt, 303 K
i-C4H10 in
MFI (silicalite-1)
Loading, q / mol kg-1
Pressure, p / Pa
0.0
0.5
1.0
1.5
2.0
10^0
10^1
10^2
10^3
10^4
10^5
10^6
10^7

Figure 4

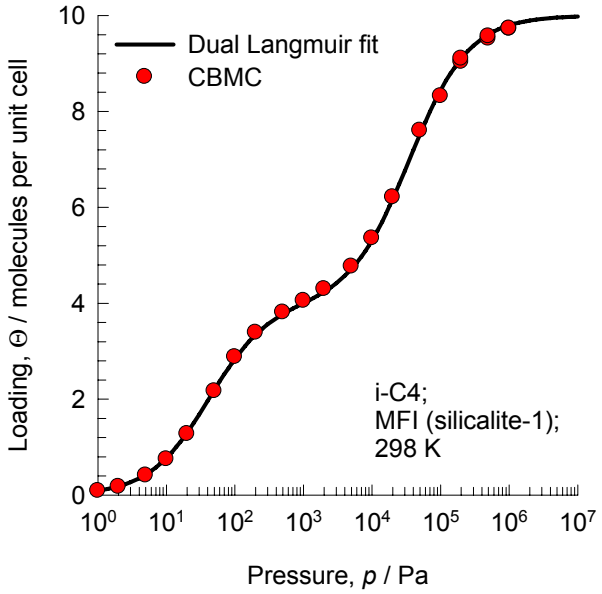
Dual Langmuir fit
CBMC
i-C4;
MFI (silicalite-1);
298 K
Loading, Θ / molecules per unit cell
Pressure, p / Pa
0
2
4
6
8
10
10^0
10^1
10^2
10^3
10^4
10^5
10^6
10^7

Figure 5

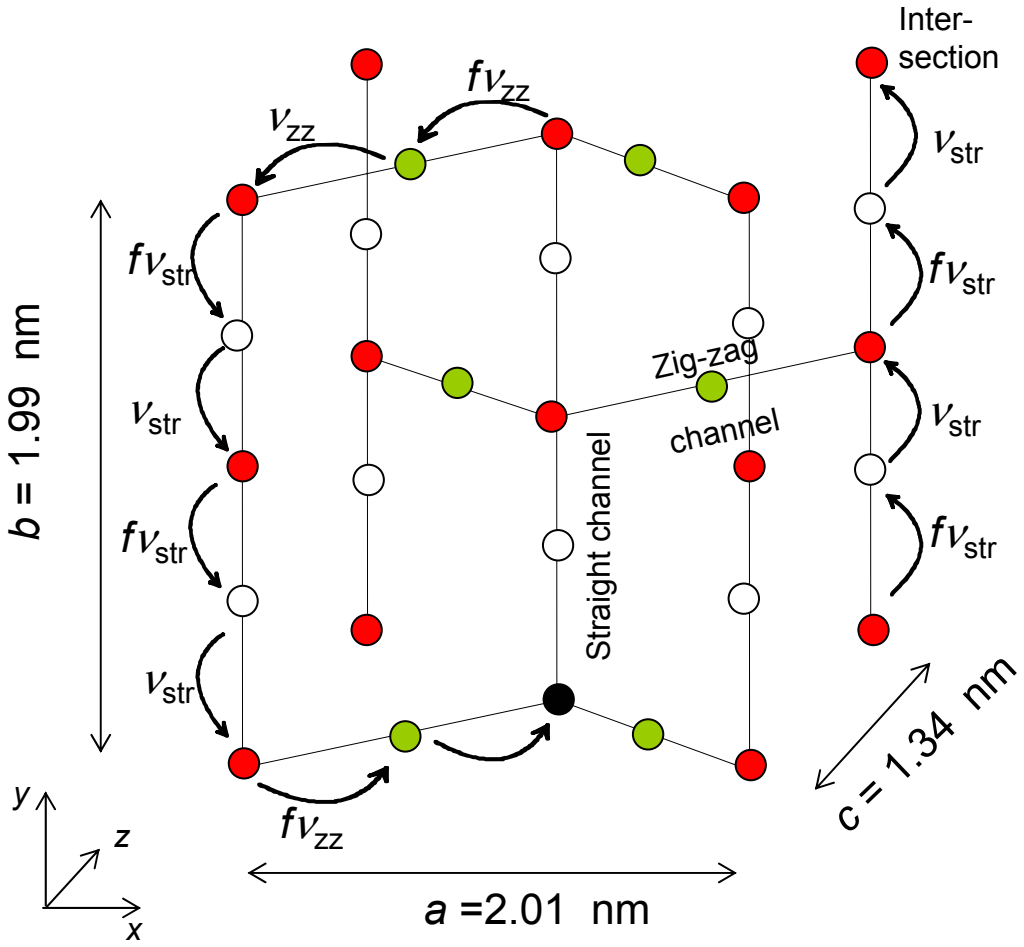

Jump frequencies chosen to match IRM experiments

$\nu_{str} = 3.5\times10^{9}\ s^{-1}$

$\nu_{zz} = 2.0\times10^{9}\ s^{-1}$

$f = 0.0012$

Kinetic Monte Carlo scheme

Figure 6